Green Chemistry

COMMUNICATION

View Article Online
View Journal | View Issue

Cite this: *Green Chem.*, 2015, **17**, 4167

Received 16th June 2015,
Accepted 30th June 2015

DOI: 10.1039/c5gc01348h

www.rsc.org/greenchem

Carboxymethyl cellulose-templated synthesis of hierarchically structured metal oxides†

Jong Wan Ko, Byung Il Lee, You Jung Chung and Chan Beum Park*

The synthesis of hierarchically structured metal oxides has been intensively pursued over many years for diverse industrial applications. Here, we report a simple but green approach for the synthesis of metal oxide fibers using carboxymethyl cellulose fibers (CMC). We synthesized 1D hierarchical metal oxides using CMC fibers as a sacrificial template. The electrostatic interaction between metal ions and carboxyl groups in CMC induced the formation of hierarchical structures of binary (*e.g.*, CeO_2, ZnO) and tertiary (*e.g.*, $CaMn_2O_4$) metal oxide fibers.

Cellulose, a main component of green plants, is the most abundant organic chemical on Earth, 10^{11} tons are produced per year in the biosphere. The polysaccharide consists of D-glucose units linked by β-1,4-glycosidic bonds and has been widely utilized in diverse engineering fields because of its biocompatibility, abundance, and high chemical stability.[1] For example, metal oxides such as TiO_2, ZnO, and Al_2O_3 had been synthesized using cellulose as a sacrificial template through simple physical adsorption of precursor metal ions on the surface of a cellulose matrix.[2] However, it was difficult to create hierarchically structured metal oxides having high crystallinity due to the limitation of controlling the interactions between precursor metal ions and the cellulose template. While the synthesis of small particulate materials with distinguished structures and high specific surface area has been intensively studied in recent years,[3] the particles often exhibit a tendency to agglomerate, causing performance degradation during their application.[4a] Hierarchically structured materials consisted of small particles with secondary structures can provide a facile pathway for efficient transfer of chemicals and electrons while maintaining active site area and unique physicochemical properties of the particles.[4]

Department of Materials Science and Engineering, Korea Advanced Institute of Science and Technology (KAIST), 335 Science Road, Yuseong-gu, Daejeon 305-701, Republic of Korea. E-mail: parkcb@kaist.ac.kr; Fax: +82 42 350 3310; Tel: +82 42 350 3340

† Electronic supplementary information (ESI) available: Experimental details and supporting data of SEM, TEM, XRD, EDX, TGA, Zeta potential measurement, FT-IR spectra, and UV-visible spectra. See DOI: 10.1039/c5gc01348h

Herein we report on the synthesis of hierarchically structured metal oxides made of nano-sized particles connected into a 1D structure with high crystallinity using carboxymethyl cellulose (CMC) as a sacrificial template. CMC possesses negatively charged carboxyl groups and high loading capacity for metal ions, such as manganese, iron, and mercury, in aqueous media.[5] The cotton-like structure of CMC fibers can facilitate the formation of porous morphologies.[5a] For example, the synthesis of magnetic mesoporous carbon composites has been reported using CMC.[6] Furthermore, CMC is a cost-effective material with good chemical stability, suitable for industrial-scale applications. We have synthesized hierarchical binary (*e.g.*, CeO_2, ZnO) and ternary metal oxides (*e.g.*, $CaMn_2O_4$) using CMC fibers according to the steps illustrated in Scheme 1a. Briefly, we incubated CMC fibers in a metal precursor solution to obtain metal ion-loaded CMC fibers through electrostatic interaction between the carboxyl groups in CMC fibers and the metal ions in the solution. Hierarchical metal oxide fibers shown in Scheme 1b were created through the calcination of metal ion-loaded CMC fibers under an air atmosphere. The synthesized metal oxide (*i.e.*, CeO_2) also showed amendable structure and macroscopic porous structure that can show low specific gravity (0.316 g cm^{-3}) (Fig. S1†). According to our analysis, the resulting hierarchically structured metal oxides and distinguished surface properties (*i.e.*, valence of metal ions) from conventional metal oxides exhibited high catalytic performances towards organic pollutant degradation, artificial photosynthesis, and oxygen reduction/evolution (Scheme 1c).

CMC fibers preferentially bind to divalent metal ions because they contain numerous hydroxyl and carboxyl groups that can chelate metal ions.[7] We considered that this property of CMC fibers could restrain particle growth during the calcination process and that an appropriate control of synthetic conditions would enable the fabrication of 1D hierarchical metal oxides. To verify the existence of Ce^{3+} ions in CMC fibers after immersion in the $CeCl_2$ solution, we conducted energy dispersive X-ray spectroscopy, zeta potential, inductively coupled plasma (ICP), and FT-IR analysis. As shown in Fig. S2,† X-ray absorption peaks corresponding to elemental

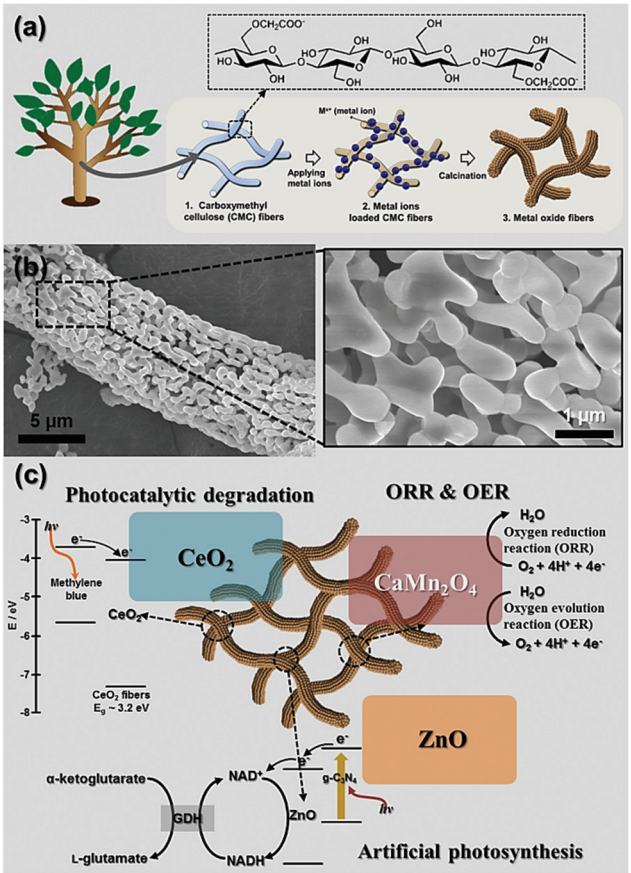

Scheme 1 (a) Schematic illustration of the synthetic process of hierarchical metal oxides using CMC fibers. (b) The SEM images of $CaMn_2O_4$ fiber with different magnification. (c) The applications of CeO_2 fibers for photocatalytic degradation of methylene blue, ZnO hybridized with g-C_3N_4 for photochemical NADH regeneration, and $CaMn_2O_4$ fibers as bi-functional electrocatalysts for the oxygen reduction reaction (ORR) and oxygen evolution reaction (OER).

Ce were observed in the Ce^{3+}-adopted CMC fibers, while SEM images exhibited no difference between pristine CMC fibers and Ce^{3+}-CMC fibers. To investigate possible electrostatic interaction between Ce^{3+} ions and carboxyl groups in CMC fibers, we analyzed the change of the surface charge of CMC fibers using zeta potential and ICP measurement after the loading of different amounts of Ce^{3+} ions. A suspension of pristine CMC fibers exhibited a zeta potential of approximately −4.76 that originated from the carboxyl groups (Fig. S3†). The value of the negative charge decreased with the increment of bound Ce^{3+} ions to the CMC fibers due to the higher number of Ce^{3+} ions bound to carboxyl groups. Cation-loading capacity of CMC fiber is known to be 1.08 meq g^{-1},[5d] which corresponds to 360 μmol of Ce^{3+} ions per gram. In this work, the amount of adsorbed Ce^{3+} ions to CMC fibers was saturated to 350 μmol of Ce^{3+} ions per gram, indicating that Ce^{3+} ions were almost fully bound to CMC fibers through electrostatic interactions. To verify the interaction between carboxyl groups and Ce^{3+} ions, we further conducted FT-IR analysis. Fig. S4a† shows FT-IR absorption peaks corresponding to the stretching vibration modes of hydroxyl groups and carboxyl groups.[8] The hydroxyl group stretching band shifted from 3450 cm^{-1} for pristine CMC fibers to 3409 cm^{-1} for Ce^{3+}-CMC fibers. This shift implies an increased intermolecular hydrogen bonding between metal ions and hydroxyl groups on the surface of CMC fibers.[8] The FT-IR spectra show the difference in the symmetric vibrational mode of carboxyl groups in CMC fibers (1415 cm^{-1}) and Ce^{3+}-CMC fibers (1324 cm^{-1}), indicating direct interaction between Ce^{3+} ions and the carboxyl groups in CMC fibers. We also modified the surface properties of CMC (*i.e.*, the extent of ionization of carboxyl groups) by protonation/deprotonation of the carboxyl groups. The FT-IR spectra are presented with peak locations and assignments (Fig. S4b†). Under acidic conditions (0.1 M HCl), the carboxyl groups on CMC were fully protonated. The carbonyl stretch[9] of carboxylic acid groups was observed at 1732 cm^{-1}. The FT-IR spectrum of basic treated CMC (1 M NaOH) is different from that at low pH. The carboxyl groups were deprotonated, as shown by the absence of a carbonyl stretch[9] at 1732 cm^{-1} and the appearance of a $-COO^-$ asymmetric stretch[9] at 1596 cm^{-1}. As shown in Fig. S5a and b,† the morphologies of CeO_2 from HCl treated CMC could not be controlled due to lower extent of deprotonated carboxyl groups. Based on high metal ion affinity of deprotonated carboxyl groups ($-COO^-$) in CMC, different morphologies of CeO_2 fibers were obtained by changing precursor concentration (Fig. S5c and d†).

We investigated the decomposition of CMC fibers and the formation of CeO_2 fibers during the calcination process. According to thermogravimetric analysis (TGA) and differential scanning calorimetry (DSC) analysis, Ce^{3+}-CMC fibers started to decompose at around 240 °C with the exothermal peak corresponding to the decomposition of cellulose at 330 °C (Fig. S6a†). The small endothermic peak at around 350 °C indicates the oxidation of Ce^{3+} ions to form CeO_2. The decomposition of residual cellulose matrix was observed with the additional exothermal peak at over 370 °C. This result suggests that the CeO_2 phase was formed before full decomposition of CMC fibers. Thus, CeO_2 fibers could retain the unique structure that consisted of interconnected nanospheres with numerous pores. The morphology of hierarchical CeO_2 fibers was significantly affected by precursor concentration and calcination temperature. According to our observation, the CeO_2 fibers with 1D hierarchical structures consisted of numerous nanospheres (~100 nm) (Fig. 1a and b) were synthesized with 4 mM $CeCl_3$ followed by calcination at 800 °C. As shown in Fig. S6b,† pore sizes in the CeO_2 fibers were distributed mostly in the range of mesopores (2–50 nm) and macropores (larger than 50 nm). Our XRD analysis confirmed the formation of a highly crystalline phase of CeO_2 by showing the corresponding X-ray diffraction pattern of CeO_2 (PDF# 43-1002) (Fig. S7a†). At lower concentration of Ce^{3+} ions (1 mM), CeO_2 fibers exhibited lower connectivity between larger CeO_2 nanoparticles (~180 nm) due to the decreased amount of Ce^{3+} ions (81.8 μmol g^{-1} according to ICP analysis) adsorbed in the CMC fibers (Fig. S8a†). When calcination was conducted at an

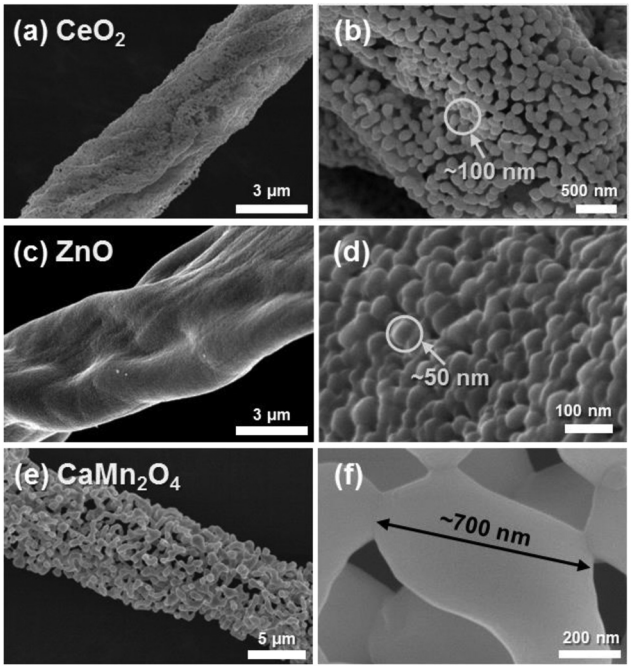

Fig. 1 SEM images of (a, b) CeO_2, (c, d) ZnO, and (e, f) $CaMn_2O_4$ with different magnification.

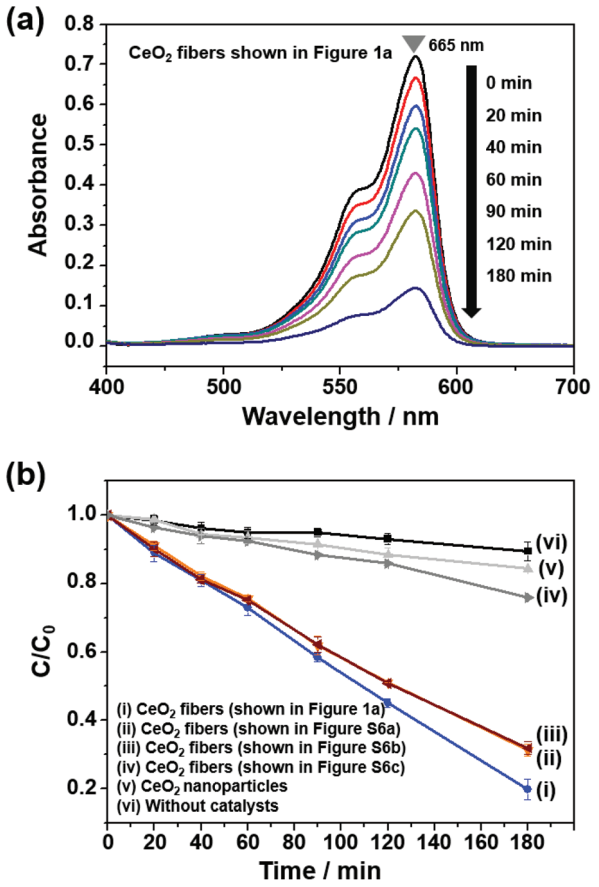

Fig. 2 (a) UV-visible spectra of MB solution monitored in the presence of CeO_2 fibers (shown in Fig. 1a) during visible light irradiation (λ > 420 nm). (b) Time profiles of MB photodegradation with (i–iv) CeO_2 fibers, (v) CeO_2 nanoparticles, and (vi) without catalyst under visible light irradiation. The change of MB concentration (C/C_0) was estimated from the intensity decrease of the absorbance at 665 nm. The error bars in the spectra represent the standard deviations of three independent measurements for each data point.

elevated temperature of 1000 °C, individual CeO_2 particles became larger (~300 nm) than those of CeO_2 fibers calcinated at 800 °C (Fig. S8b†) due to the thermodynamic facilitation of particle growth at high temperature. Denser CeO_2 fibers with pores on the smooth surface were obtained at higher Ce^{3+} ion concentration (20 mM) (Fig. S8c†). The type of metal elements also influenced the resulting structure of metal oxides; while ZnO fibers also consisted of spherical, crystalline ZnO nanoparticles (~50 nm) and numerous pores (<10 nm) (Fig. 1c and d, and S7b†), they exhibited a pleated surface and denser 1D structure than that of CeO_2 fibers (Fig. 2c and d). $CaMn_2O_4$, a ternary metal oxide, had submicron-sized granules (~700 nm) of a highly crystalline phase of $CaMn_2O_4$ (PDF# 70-4889) connected into fibers (Fig. 1e and f, and S7c†). The void and particle size in the $CaMn_2O_4$ fibers varied depending on the amount of CMC fibers in the precursor solution (Fig. S9a and b†). With a higher amount of CMC fibers (120 mg mL^{-1}), $CaMn_2O_4$ particles were readily formed with approximate size of 700 nm due to the insufficiency of ion concentration (Ca 10.3 μmol g^{-1}; Mn 22.8 μmol g^{-1}) in CMC fibers for the formation of fibrous $CaMn_2O_4$ (Fig. S9c†). This result indicates that the density of adopted metal ions in CMC fibers influences the final morphology of $CaMn_2O_4$, similar to the formation of CeO_2 fibers.

We investigated the catalytic activities of the thus-synthesized hierarchical metal oxides for photocatalysis, artificial photosynthesis, and electrocatalysis. We evaluated the activity of hierarchically structured CeO_2 fibers by measuring photocatalytic degradation of methylene blue (MB). Fig. 2a shows the change in UV-visible absorption spectrum of MB in the presence of CeO_2 fibers shown in Fig. 1a under visible light (λ > 420 nm). The absorption peak continued to decline with visible light illumination, and approximately 80% of MB was degraded within 3 hours. To compare the rate of MB degradation with that by CeO_2 nanoparticles (<25 nm, BET surface area 34.16 m^2 g^{-1}) (Fig. S10 and S11†), we plotted the time profiles of normalized concentration (C/C_0) change from the normalized absorbance (A/A_0) at 665 nm (Fig. 2b). Despite the smaller specific surface area of CeO_2 fibers (0.24–3.17 m^2 g^{-1}) than that of CeO_2 nanoparticles (34.16 m^2 g^{-1}), CeO_2 fibers showed much enhanced photocatalytic activity than CeO_2 nanoparticles. The highest value of rate constant (k) for MB degradation by the CeO_2 fibers was calculated to be 1.05×10^{-2} min^{-1}, which was 20-fold higher than that by CeO_2 nanoparticles ($k = 0.046 \times 10^{-2}$ min^{-1}). In the photodegradation of MB molecules, photo-excited electrons at the LUMO level of MB (−3.60 V)[10] needs to be transferred to the conduction band of CeO_2 (−4.06 V).[11] The oxidative forms of MB then become a

cationic radical that takes part in self-degradation. Moreover, CeO_2 catalytically reduces oxygen to reactive oxygen species (*i.e.*, hydroxyl radical) which can oxidize and decolorize MB molecules.[12] The catalytic activity for hydroxyl radical generation can be significantly increased by higher concentration of Ce^{3+} ions on CeO_2 surface.[13] X-ray photoelectron spectroscopy (XPS) analysis was conducted in order to characterize the valence state of cerium in CeO_2 samples. For Ce 3d XPS spectrum of CeO_2 fibers, the ratio of peaks corresponding to the Ce^{3+} state (885.2 and 902.2 eV) is higher than those of CeO_2 nanoparticles (10.4 mol% for CeO_2 fibers; 4.8 mol% for CeO_2 nanoparticles) (Fig. S12†). The improved photocatalytic performance of CMC-templated CeO_2 fibers should stem from the high concentration of Ce^{3+} ions by producing reactive oxygen species (*e.g.*, hydroxyl radical), which could degrade MB molecules. We determined the hydroxyl radical ($OH^{\bullet}$), which could accelerate the MB degradation reaction, by measuring the fluorescent 2-hydroxyl terephthalate (TA-$OH^{\bullet}$) using fluorescence spectroscopy. As shown in Fig. S13,† the photoluminescence intensity of TA-$OH^{\bullet}$ at 425 nm increased during photocatalytic MB degradation with CeO_2 fibers, while TA-$OH^{\bullet}$ was not observed with CeO_2 nanoparticles (Fig. S13 inset†).

Recently, ZnO had been extensively studied for solar energy harvesting due to its high electronic mobility and good chemical stability.[14] We analyzed the light harvesting capability of 1D hierarchical ZnO fibers toward biocatalyzed artificial photosynthesis that aims for the visible light-driven regeneration of NAD(P)H coupled with the redox enzymatic reaction.[15] Since ZnO has a large bandgap (3.1 eV) to absorb mostly UV light, we utilized graphitic carbon nitride (g-C_3N_4) as a visible light-active material (Fig. S14†). The composite of g-C_3N_4 sheets and ZnO fibers (g-C_3N_4/ZnO fibers) was prepared by a simple mixing and evaporation method (Fig. 3a and S15†). As illustrated in Fig. S16,† g-C_3N_4 can absorb visible light and generate electrons in its conduction band (−1.12 V *vs.* NHE),[16] and photo-excited electrons are transferred to ZnO fibers due to the more positive position of the conduction band edge of ZnO compared to g-C_3N_4 (at least 0.4 V more positive), thereby regenerating NADH in conjunction with redox enzymatic synthesis of L-glutamate from α-ketoglutarate. The NADH regeneration rate by g-C_3N_4/ZnO fibers was 5.25 μmol g^{-1} $hour^{-1}$, which was eight times higher than that of g-C_3N_4/ZnO nanoparticles (0.63 μmol g^{-1} $hour^{-1}$) (Fig. 3b). We attribute the increased NADH regeneration rate of g-C_3N_4/ZnO fibers to the hierarchical morphology that provides facile electron transfer between g-C_3N_4 and ZnO fibers. As shown in Fig. S17,† in the case of g-C_3N_4/ZnO fibers, higher photocurrent response than those of bare g-C_3N_4 and g-C_3N_4/ZnO nanoparticles was observed, which means that superior photo-activity of g-C_3N_4/ZnO fibers under visible light irradiation. By coupling NADH photoregeneration with redox enzymatic reaction of L-glutamate dehydrogenase (GDH), L-glutamate was successfully produced under visible light (Fig. 3c).

We found that the hierarchical $CaMn_2O_4$ fibers have high potential for electrocatalytic applications for the oxygen

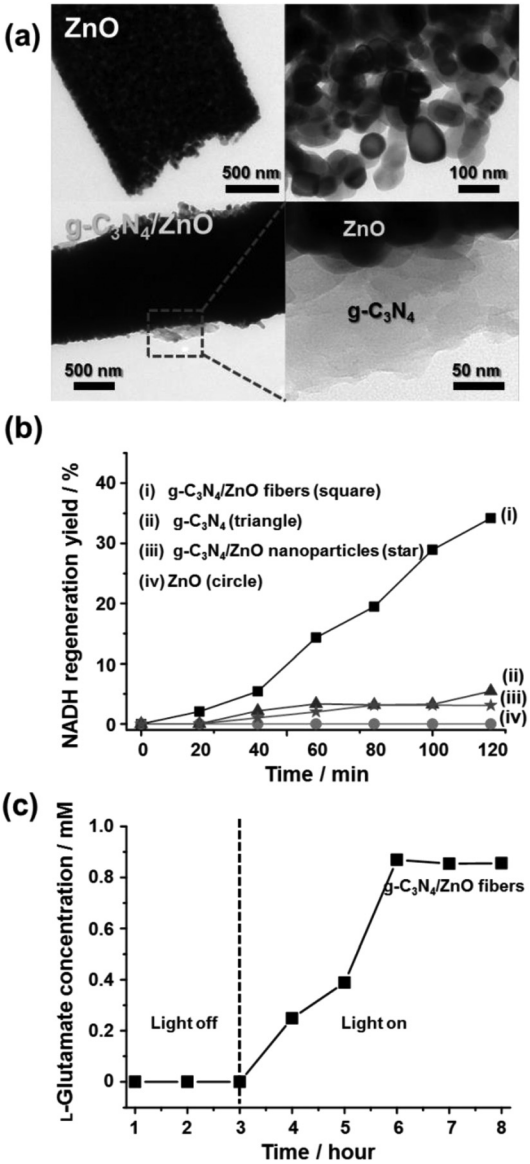

Fig. 3 (a) TEM images of ZnO fiber and g-C_3N_4/ZnO composite fiber with different magnification. (b) Photochemical NADH regeneration of g-C_3N_4/ZnO fibers, g-C_3N_4, g-C_3N_4/ZnO nanoparticles, and ZnO fibers under visible light irradiation (λ > 420 nm). (c) Photoenzymatic conversion of α-ketoglutamate to L-glutamate with g-C_3N_4/ZnO composite was conducted after 3 hour of the dark reaction in NADH regeneration.

reduction (ORR) and evolution reactions (OER). Manganese-based oxides have been widely studied for energy storage and catalysis due to the advantages of cost efficiency, high abundance, and low toxicity.[17] We examined electrocatalytic activity of $CaMn_2O_4$ fibers for bi-functional reactions of ORR and OER. We considered that the distinctive structure of hierarchical $CaMn_2O_4$ fiber would prevent crystalline $CaMn_2O_4$ particles from agglomeration that can inhibit electrochemical performance. As a control, we prepared bulk $CaMn_2O_4$ by a conventional hydrothermal process (Fig. S18†). When we analyzed electrocatalytic activities of $CaMn_2O_4$ for ORR and OER using

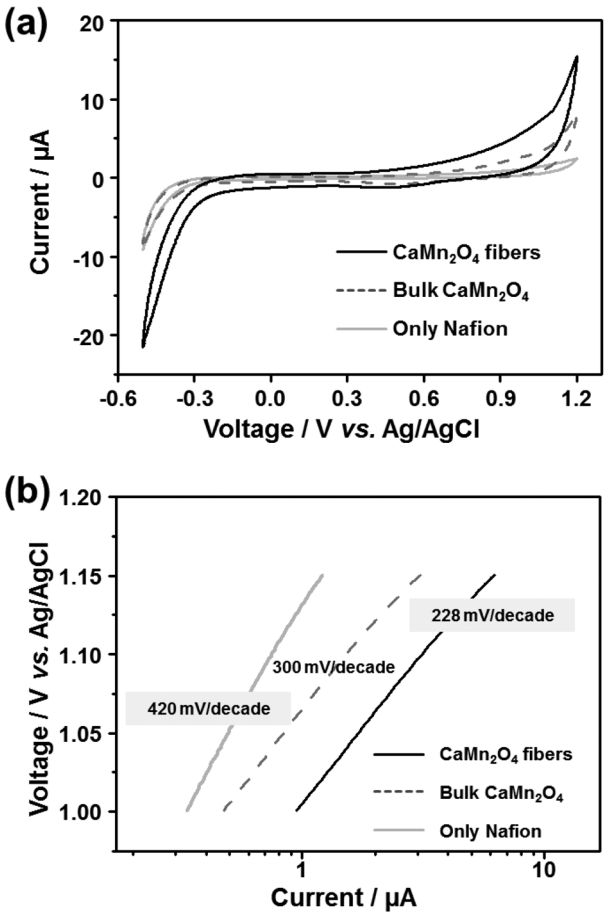

Fig. 4 (a) Cyclic voltammetry curves of $CaMn_2O_4$ fibers (black solid line), bulk $CaMn_2O_4$ (grey dash line), and only Nafion (grey solid line) in 0.1 M phosphate buffer solution (pH 7.0) saturated with O_2. (b) The plots of Tafel slope of OER current in (b).

cyclic voltammetry (CV), cathodic current of $CaMn_2O_4$ fibers was observed at −0.327 V (Fig. 4a), which was much lower than those of bulk $CaMn_2O_4$ (−0.443 V) and Nafion-coated glassy carbon (−0.449 V) electrodes. The cathodic current of $CaMn_2O_4$ fibers indicates a facile electrocatalytic reaction of O_2 reduction in aqueous media. In the oxidation range of cyclic voltammetric analysis, the $CaMn_2O_4$ fiber electrode showed an anodic current of 5 μA at a lower overpotential (0.349 V) than that of bulk $CaMn_2O_4$ (0.512 V). The hierarchical $CaMn_2O_4$ fibers exhibited much smaller Tafel slope decrease (228 mV per decade) than that (300 mV per decade) of bulk $CaMn_2O_4$ (Fig. 4b). The smaller Tafel slope of $CaMn_2O_4$ fibers indicates faster electron transfer during OER. Although Ca is considered to be inactive in redox reaction such as ORR and OER.[18] In photosystem II (PS II) oxygen evolution center, Ca is considered as a critical cofactor for the OER, as providing an active and binding site for oxygen-containing species.[18] For this reason, we analyzed the state of Ca in $CaMn_2O_4$ samples using XPS. (Fig. S19†) In the case of $CaMn_2O_4$ fibers, the typical Ca 2p peak (346.5 eV) and lower binding energy peak (345.1 eV) are observed, while similar spectra of Mn 2p were obtained from both $CaMn_2O_4$ samples. The difference in the Ca 2p state, which correlated with the shift of the O 1s peak toward a lower binding energy (from 529.7 to 529.0 eV), could affect behaviors (*i.e.*, attachment and activation) of oxygen species[19] and would facilitate the ORR and OER reaction of $CaMn_2O_4$ fibers. In addition, the enhanced bi-functional electrocatalytic performance of $CaMn_2O_4$ fibers is also attributed to their hierarchical structure that enables facile mass transfer for ORR and OER. Our results show bi-functional electrocatalytic activity of the $CaMn_2O_4$ fibers, unlike bulk $CaMn_2O_4$; electrocatalytic OER activity of $CaMn_2O_4$ is reported for the first time in this work.

Conclusions

Metal oxides have attracted high attention in the past decades due to their distinct photocatalytic and electrical activities with high chemical, thermal, and mechanical stabilities. In this work, we have demonstrated the utility of CMC fibers as a sacrificial template to produce binary and tertiary metal oxide fibers. The electrostatic interaction between metal ions and the carboxyl groups in CMC fibers induced a hierarchical structure of metal oxides. The morphologies of synthesized metal oxides (*e.g.*, CeO_2, ZnO, and $CaMn_2O_4$) could be controlled according to synthetic conditions, such as metal precursor concentration, calcination temperature, and the amount of CMC fibers. Thus-synthesized CMC-templated metal oxide fibers exhibited enhanced performances for photocatalytic, photochemical, and electrocatalytic reactions. The CeO_2 fibers showed much higher photocatalytic activity than CeO_2 nanoparticles due to superior ability to generate reactive oxygen species which can degrade organic pollutants. We also demonstrated that hierarchical ZnO fibers hybridized with g-C_3N_4 could provide a directional charge transfer pathway and showed their utility for biocatalyzed artificial photosynthesis through visible light-driven chemical NADH regeneration coupled with a redox enzymatic reaction. The electrochemical properties of $CaMn_2O_4$ fibers enabled bi-functional reactions of ORR and OER. We expect that this economical and environmentally friendly approach could be extended to the green synthesis of hierarchically structured materials of other metal oxides.

Acknowledgements

This study was supported by grants from the National Research Foundation (NRF) *via* the National Leading Research Laboratory (NRF-2013R1A2A1A05005468) and the Intelligent Synthetic Biology Center of Global Frontier R&D Project (2011-0031957), Republic of Korea.

Notes and references

1 (*a*) R. J. Moon, A. Martini, J. Nairn, J. Simonsen and J. Youngblood, *Chem. Soc. Rev.*, 2011, **40**, 3941;

(*b*) I. Delidovich, K. Leonhard and R. Palkovits, *Energy Environ. Sci.*, 2014, **7**, 2803; (*c*) A. S. Amarasekara and O. S. Owereh, *Ind. Eng. Chem. Res.*, 2009, **48**, 10152; (*d*) P. Laaksonen, A. Walther, J.-M. Malho, M. Kainlauri, O. Ikkala and M. B. Linder, *Angew. Chem., Int. Ed.*, 2011, **50**, 8688.

2 (*a*) J. Huang and Y. Gu, *Curr. Opin. Colloid Interface Sci.*, 2011, **16**, 470; (*b*) E. Ghadiri, N. Taghavinia, S. M. Zakeeruddin, M. Gratzel and J.-E. Moser, *Nano Lett.*, 2010, **10**, 1632; (*c*) J. T. Korhonen, P. Hiekkataipale, J. Malm, M. Karppinen, O. Ikkala and R. H. A. Ras, *ACS Nano*, 2011, **5**, 1967.

3 (*a*) M. Gu, I. Belharouak, A. Genc, Z. Wang, D. Wang, K. Amine, F. Gao, G. Zhou, S. Thevuthasan, D. R. Baer, J. G. Zhang, N. D. Browning, J. Liu and C. Wang, *Nano Lett.*, 2012, **12**, 5186; (*b*) C. He, A. J. Grutter, M. Gu, N. D. Browning, Y. Takamura, B. J. Kirby, J. A. Borchers, J. W. Kim, M. R. Fitzsimmons, X. Zhai, V. V. Mehta, F. J. Wong and Y. Suzuki, *Phys. Rev. Lett.*, 2012, **109**, 197202.

4 (*a*) Y. Ren, Z. Ma and P. G. Bruce, *Chem. Soc. Rev.*, 2012, **41**, 4909; (*b*) A. Q. Pan, H. B. Wu, L. Zhang and X. W. Lou, *Energy Environ. Sci.*, 2013, **6**, 1476.

5 (*a*) J. D. Reid and G. C. Daul, *Text. Res. J.*, 1949, **19**, 794; (*b*) A. B. Bourlinos and D. Petridis, *Chem. Commun.*, 2002, 2788; (*c*) Y. Gong, Y. Liu, Z. Xiong and D. Zhao, *Environ. Sci. Technol.*, 2014, **48**, 3986; (*d*) S. Yang, S. Fu, H. Liu, Y. Zhou and X. Li, *J. Appl. Polym. Sci.*, 2010, **119**, 1204; (*e*) Y. Zhang, Y. Liu, X. Wang, Z. Sun, J. Ma, T. Wu, F. Xing and J. Gao, *Carbohydr. Polym.*, 2014, **101**, 392.

6 (*a*) Q. Wu, W. Li, J. Tan, X. Nan and S. Liu, *Appl. Surf. Sci.*, 2015, **332**, 354; (*b*) Q. Wu, W. Li, J. Tan and S. Liu, *RSC Adv.*, 2014, **4**, 61518; (*c*) D. Yamaguchi, K. Furukawa, M. Takasuga and K. Watanabe, *Sci. Rep.*, 2014, **4**, 6053.

7 (*a*) X. Zhao, L. Lv, B. Pan, W. Zhang, S. Zhang and Q. Zhang, *Chem. Eng. J.*, 2011, **170**, 381; (*b*) J. Wang, X. Lin, X. Luo and Y. Long, *Chem. Eng. J.*, 2014, **252**, 415; (*c*) N. C. Cady, J. L. Behnke and A. D. Strickland, *Adv. Funct. Mater.*, 2011, **21**, 2506.

8 F. He, D. Zhao, J. Liu and C. B. Roberts, *Ind. Eng. Chem. Res.*, 2006, **46**, 29.

9 L. T. Cuba-Chiem, L. Huynh, J. Ralston and D. A. Beattie, *Langmuir*, 2008, **24**, 8036.

10 J. S. Lee, K. H. You and C. B. Park, *Adv. Mater.*, 2012, **24**, 1084.

11 J. W. Ko, J. H. Kim and C. B. Park, *J. Mater. Chem. A*, 2013, **1**, 241.

12 D. Channei, B. Inceesungvorn, N. Wetchakun, S. Ukritnukun, A. Nattestad, J. Chen and S. Phanichphant, *Sci. Rep.*, 2014, **4**, 5757.

13 C. T. Campbell and C. H. F. Peden, *Science*, 2005, **309**, 713.

14 Q. Zhang, C. S. Dandeneau, X. Zhou and C. Cao, *Adv. Mater.*, 2009, **21**, 4087.

15 (*a*) S. H. Lee, J. H. Kim and C. B. Park, *Chem. – Eur. J.*, 2013, **19**, 4392; (*b*) J. H. Kim, D. H. Nam and C. B. Park, *Curr. Opin. Biotechnol.*, 2014, **28**, 1; (*c*) J. Ryu, S. H. Lee, D. H. Nam and C. B. Park, *Adv. Mater.*, 2012, **24**, 1084; (*d*) J. Ryu, D. H. Nam, S. H. Lee and C. B. Park, *Chem. – Eur. J.*, 2014, **20**, 12020; (*e*) S. H. Lee, D. H. Nam, J. H. Kim, J.-O. Baeg and C. B. Park, *ChemBioChem*, 2009, **10**, 1621; (*f*) J. H. Kim, M. Lee and C. B. Park, *Angew. Chem., Int. Ed.*, 2014, **53**, 6364; (*g*) J. H. Kim, M. Lee, J. S. Lee and C. B. Park, *Angew. Chem., Int. Ed.*, 2012, **51**, 517; (*h*) M. Lee, J. U. Kim, J. S. Lee, B. I. Lee, J. Shin and C. B. Park, *Adv. Mater.*, 2014, **26**, 4463.

16 Y. Wang, R. Shi, J. Lin and Y. Zhu, *Energy Environ. Sci.*, 2011, **4**, 2922.

17 (*a*) Y. Liang, H. Wang, J. Zhou, Y. Li, J. Wang, T. Regier and H. Dai, *J. Am. Chem. Soc.*, 2012, **134**, 3517; (*b*) F. Cheng, J. Shen, B. Peng, Y. Pan, Z. Tao and J. Chen, *Nat. Chem.*, 2011, **3**, 79; (*c*) Y.-K. Sun, M.-J. Lee, C. Yoon, J. Hassoun, K. Amine and B. Scrosati, *Adv. Mater.*, 2012, **24**, 1192; (*d*) Y. Cao, L. Xiao, W. Wang, D. Choi, Z. Nie, J. Yu, L. Saraf, Z. Yang and J. Liu, *Adv. Mater.*, 2011, **23**, 3155.

18 (*a*) X. Han, T. Zhang, J. Du, F. Cheng and J. Chen, *Chem. Sci.*, 2013, **4**, 368; (*b*) C. F. Yocum, *Coord. Chem. Rev.*, 2008, **252**, 296.

19 M. Wiechen, I. Zaharieva, H. Dau and P. Kurz, *Chem. Sci.*, 2012, **3**, 2330.

